

Kilohertz laser ablation for doping helium nanodroplets

M. Mudrich,* B. Forkl, S. Müller, M. Dvorak, O. Bünermann, and F. Stienkemeier
Physikalisches Institut, Universität Freiburg, D-79104 Freiburg, Germany.

(Dated: February 8, 2022)

A new setup for doping helium nanodroplets by means of laser ablation at kilohertz repetition rate is presented. The doping process is characterized and two distinct regimes of laser ablation are identified. The setup is shown to be efficient and stable enough to be used for spectroscopy, as demonstrated on beam-depletion spectra of lithium atoms attached to helium nanodroplets. For the first time, helium droplets are doped with high temperature refractory materials such as titanium and tantalum. Doping with the non-volatile DNA basis Guanine is found to be efficient and a number of oligomers are detected.

I. INTRODUCTION

Helium nanodroplet isolation (HENDI) has established as a versatile technique for spectroscopic studies of a variety of atomic and molecular systems, ranging from microwave and infrared spectroscopy of small molecules to electronic spectroscopy of molecular complexes [1]. In particular the property of helium droplets to efficiently cool dopant particles down to 0.4 K equilibrium temperature and to act as nanoscale reactors for assembling molecular complexes of virtually any constituents has stimulated studies of rather unconventional molecular systems [2, 3]. Recent directions include larger metal clusters [4] and studies of the dynamics of doped helium droplets [5].

Up to now, the choice of dopants has mostly been constrained by the limited possibilities to bring molecules into the gas phase by thermal evaporation inside a heated cell. Therefore, only a restricted number of metals and larger organic molecules have found their way into helium droplet machines [6]. Using a pyrolysis source, the range of dopant molecules has been extended to radicals [7]. However, the study of metal clusters including elements such as Fe, Ni, Co, Ti, V, Nb, Au, Pt is of considerable interest for their particular magnetic or superconducting properties at very low temperatures and for their catalytic properties. Furthermore, the ability of doping fragile organic molecules would extend the study of spectra of biomolecules at 0.4 K and the optic properties of organic aggregates, the latter being of particular interest in the context of organic opto-electronic devices. Moreover, doping helium droplets with ions, as demonstrated using laser ablation [8], opens up a new class of experiments. Besides the spectroscopic interest in ions inside doped helium droplets [9], ion doped droplets will enable experiments with size-selected helium droplets.

Different variants of laser ablation sources have been developed for different applications. Generally, two regimes of interaction of laser radiation with solid material can be distinguished. In the regime of intermedi-

ate power densities, laser desorption/vaporization leads to the removal of neutral molecules from the surface. The surface may consist of bulk sample material, of a monolayer of transparent sample on a strongly absorbing metal substrate [10] or of a thick, strongly absorbing matrix in which a small amount of sample material is doped [11]. Laser desorption/vaporization is of relevance for vaporizing large, fragile molecules such as proteins and DNA for gas-phase analysis [12]. In the regime of high laser power densities, non-thermal processes lead to ejection or ablation of material into the gas-phase involving complex laser-plasma interaction processes. The latter regime is particularly interesting as a source of inorganic and metallic clusters [13, 14, 15, 16, 17, 18] and of free electrons and ions [8, 19].

The combination of laser desorption with supersonic jets is a widely used technique for several reasons. Laser desorbed molecules are translationally and internally very hot and are likely to fragment unless they are cooled by thermalization with cold carrier gas in the expansion [20]. Furthermore, the molecules are formed in sufficient abundance and with sufficient shot-to-shot stability to do spectroscopy.

The combination of laser ablation/desorption with a helium droplet beam source has been reported before only by Ghazarian and co-workers and by our group [8, 19]. However, in the experiment of Ref. [19] droplet formation occurs by postexpansion condensation in a high density helium atmosphere, which is quite different compared to a nanodroplet beam traveling under high vacuum conditions [8]. As with standard molecular beam machines, the laser ablation target is placed next to the jet expansion to benefit from the high thermalization rate of ablated particles with high density helium gas. In a second stage, the atoms or molecules picked up by the helium droplets are further cooled to the equilibrium temperature of 0.4 K through evaporation of helium atoms off the droplets.

The motivation for setting up a stable laser-ablation source with kilohertz repetition rate is manifold. Since laser-ablation sources are not inherently very stable, extensive signal averaging is generally required. On the one hand, many applications such as coincidence measurements require small signal rates per laser shot. The only way of reducing the measuring time is to increase the

*Electronic address: mudrich@physik.uni-freiburg.de

repetition rate of the experimental cycles. On the other hand, in applications in which large particle fluxes are needed such as mass-selected deposition on surfaces, up-scaling the repetition rate increases the efficiency which saves time or allows to study species of low abundance. Furthermore, modern nanosecond and femtosecond laser systems are typically operated at 1 kHz or higher repetition rate. Ideally, the laser ablation source should match the repetition rate of the laser system. The laser-ablation source presented in this article has been developed to eventually combine it with a fs-laser system and a pulsed beam of helium nanodroplets, each being operated at 1 kHz repetition rate.

In this paper we demonstrate the stable operation of a laser ablation source at kilohertz repetition rate for doping a beam of helium nanodroplets (He_N , $N \sim 10^4$) with refractory materials and biomolecules. Doping helium droplets with ions using laser ablation has been demonstrated before [8]. In the following, the design of the simple yet versatile mechanical setup is detailed. A load-lock system is implemented for exchanging samples without breaking the vacuum. This is crucial when operating a low temperature droplet source where venting costs considerable time, generally a day. The process of doping helium nanodroplets by laser ablation is characterized using lithium (Li) and magnesium (Mg) as sample materials. Long-term stability is shown to be high enough to perform laser spectroscopy of laser ablated Li atoms. The applicability of the new laser ablation source to doping with high temperature refractory metals and with the non-volatile DNA base guanine is demonstrated.

II. EXPERIMENT

The laser ablation setup is incorporated into the source chamber of a helium droplet machine, which is described in detail elsewhere [8, 21]. In short, helium gas (stagnation pressure 30-60 bar) expands through a cold (14-20 K) nozzle 10 μm in diameter. Behind the skimmer (diameter: 400 μm , distance: 16 mm) the droplet beam passes through a heated cell for doping with Li atoms in order to compare with doping by laser ablation. Further downstream the doped droplet beam is analysed using a commercial quadrupole mass spectrometer (QMS) with an electron impact ionizer (Extrel, mass range 1-1000 amu). Furthermore, a Langmuir-Taylor surface ionization detector terminates the doped droplet beam. This detector can accurately measure the number of alkali and alkaline earth doped helium droplets [22].

The advantages of implementing the laser ablation setup directly into the source chamber are the following: First, this compact geometry allows to produce a beam of doped helium droplets in only one vacuum chamber. Second, laser ablated atoms and molecules carry a large amount of kinetic and internal energy. They are efficiently “precooled” by scattering with the relatively high density of helium atoms in the outer parts of beam. In

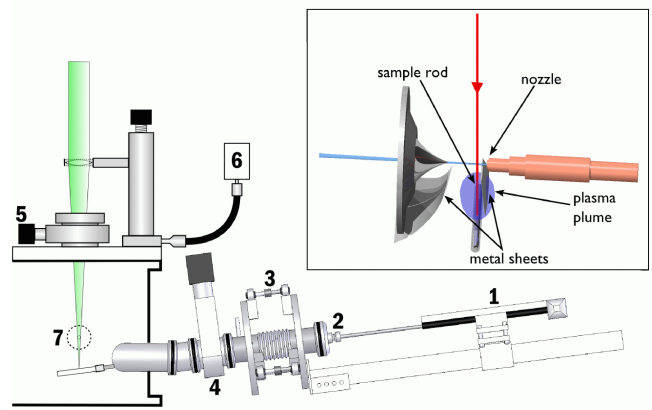


FIG. 1: Side view of the mechanical setup for implementing kHz laser ablation into the helium droplet machine. The ablation laser beam enters the nozzle chamber from above through an entrance window mounted on a gate valve (5) and is focused onto the sample rod. The helium droplet beam propagates normal to the paper plane through the skimmer (dashed circle, (7)) right above the target rod. The main technical features are (1) a translation stage mounted upside down, (2) a rotary feedthrough, (3) a bellow chamber serving as vacuum lock and for aligning the sample, (4, 5) gate valves, and (6) a motor coupled to a translation stage which moves the focusing lens back and forth. The inset shows the metal sheets that cover the direct line of sight from the ablation spot to nozzle and skimmer orifices.

this way, internal and kinetic energies are sufficiently reduced for the particles to attach to helium droplets without complete evaporation of the droplets. Furthermore, the laser ablated particles can directly serve as seeds and enhance droplet condensation. This effect has been observed in the case of doping with atomic ions [8].

The laser ablation setup is depicted in Fig. 1. A target rod (3-10 mm in diameter, up to 7 cm length) is placed ≈ 2 cm below the helium beam in between the cryogenic nozzle and skimmer perpendicularly to the droplet beam. The vertical position corresponds to a distance of the sample from the droplet beam causing negligible interferences with the beam expansion. However, moving the vertical position of the sample in the range of ± 10 mm has only little influence on the laser doping efficiency. A focused laser beam enters the source chamber from above through a window and creates an ablation plume on the target surface which is directed towards the helium beam. In order to homogeneously ablate the entire rod surface the sample rod is simultaneously translated and rotated along its axis in a helical fashion. In this way, a new sample spot is provided to each laser pulse in order to minimize the formation of grooves. This is realized by coupling the rod to the spindle of a commercial motorized translation stage mounted upside down onto its moving stage outside the vacuum chamber (label (1) in Fig. 1). At the endpoints of the translational stage, the direction of motion is reversed and helical motion of the opposite sense occurs. The translational stage (OWIS,

model X41.083.101 GP) has a travel range of 95 mm at a spindle pitch of 0.5 mm and is operated at about 200 revolutions per minute. The 520 mm long connecting shaft transmits the mechanical motion into the vacuum chamber through a commercial rotary feedthrough designed for high rotation frequencies and stable guiding of the shaft (K. Lesker) (2). It is coupled to the spindle of the translation stage and to the sample rod by stiff couplers. Precise alignment of the axis of the translation stage and the feedthrough is an important issue since, due to the considerable length of the shaft, a slight misalignment results immediately in an unbalanced motion at the laser intersection point. The sample rod can be aligned with respect to nozzle and skimmer using three fine thread screws connecting two steel plates by ball joints (3). The steel plates are welded onto the flanges of a bellow, which serves as vacuum lock chamber for rapid exchange of the sample rods. The translational stage is mounted onto a slider which can be moved along a four cornered aluminium shaft such that the sample can be pulled out into the bellow chamber. The whole setup is attached to the source chamber by a manual gate valve (4). In order to compensate the torque acting onto the flange the four cornered shaft is supported at its end by a spring.

Previous experiments on laser ablation have shown that clogging of the $10\text{ }\mu\text{m}$ -nozzle and the 0.4 mm skimmer is a severe drawback in particular when working at high repetition rates. Various geometries have been tested for shielding nozzle and skimmer from the vapor expanding out of the ablation plume. Our attempts included sheathing the sample rod with a metal cylinder with a slit along its axis allowing the laser to interact with the sample surface. However, no unperturbed ablation conditions were achieved using this type of shielding. The best results are obtained by placing small sheet metal strips underneath nozzle and skimmer such that the direct line of sight from the laser-surface interaction region to nozzle and skimmer orifices is covered without affecting the helium jet.

The ablation laser is a pulsed frequency-doubled Nd:YLF laser (526 nm) that produces pulse energies of up to 15 mJ at 1 kHz repetition rate (Quantronix Falcon 263). The pulse duration is in the range 130 - 250 ns depending on laser power. A few measurements for characterizing laser doping at pulse energies exceeding 15 mJ are performed using a Nd:YAG laser (1064 nm) at 10 Hz repetition rate (Quanta-Ray) with pulse lengths of about 10 ns. Although the laser wavelengths and pulse durations are different, no significant differences in the laser ablation efficiency have been observed.

The laser beam is focused onto the sample rod using a lens of 300 mm focal length which is mounted on a x -, y -, and z -translation stage. In vertical direction the lens position can be varied in a range of 50 mm in order to change the energy density and the ablation spot size. The horizontal alignment is important to center the laser beam focus on the metal rod in between nozzle and skimmer. Following M. Smits and coworkers [23], the lens is

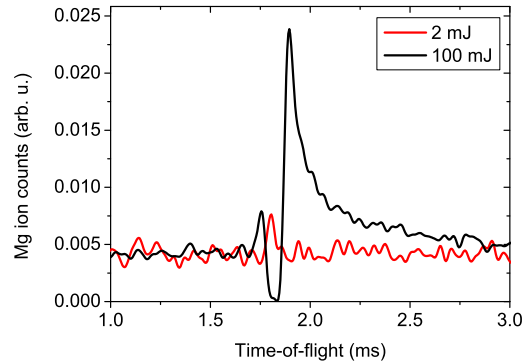


FIG. 2: Time-of-flight signal traces of helium nanodroplets doped with Mg for two different laser pulse energies of the Nd:YAG laser operated at 10 Hz repetition rate. The signal is measured using a quadrupole mass spectrometer set to a mass of 24 amu.

periodically moved back and forth by 0.5 mm in order to avoid the formation of grooves on the sample rod and thus to improve long-term stability of the ablation signal. This is done by connecting a small DC-motor to the x -translation stage via a flexible shaft ((6) in Fig. 1). Both controllers for this motor and for the motorized translation stage are home built.

Although the laser entrance window is situated 240 mm above the ablation sample, considerable coating of the window surface is an issue when working with metal samples. Depending on the type of metal used, the coating leads to strong absorption of the laser light and to noticeable heating of the window. This has even lead to cracking of the window. For this reason, a thickness of the laser entrance window of 6 mm or thicker should be chosen. In order to enable rapid exchange of the window for cleaning or replacement a manual gate valve is introduced in between the vacuum chamber and the window mount (5). This deficiency may resolved by shielding the window with a gas buffer (see e.g. Ref. [23]).

III. DOPING HELIUM NANODROPLETS BY LASER ABLATION

A. Laser ablation of magnesium

When using laser ablation as means of doping a helium nanodroplet beam, the desired process of attaching atoms or ions to the droplets competes with an unwanted effect of the ablation plume on the droplet beam: depletion of the beam by inelastic collisions of the droplets with high-energetic particles at high density.

The competition between doping and beam destruction is apparent when comparing the detector signals recorded as a function of delay time after the laser pulse for low

(2 mJ) and high (100 mJ) pulse energies, as depicted in Fig. 2. Similar signal traces for ablation of sodium and magnesium have been discussed in detail in Ref. [8]. The shown signal traces reflect doping by ablation of Mg using a Nd:YAG laser (1064 nm) operated at 10 Hz repetition rate. The laser beam is focused to a waist of 0.2 mm. In this experiment a QMS with electron impact ionization at 30 eV electron energy is used as a detector. The detector is operated in pulse counting mode and the detector pulses are discriminated and recorded using a multi-channel scaler. The response time of the QMS is in the range 30–40 μ s which leads to a small broadening effect on the time structure of the signal.

The ion signal shown in Fig. 2 reflects the number of ion counts per 10 μ s time bin and per laser shot measured with our QMS detector. Since the measured count rate strongly depends on the particular detector used it should by no means be mistaken as an absolute value of the beam intensity. The absolute intensity of doped helium droplets is roughly estimated to be a factor 10^5 larger than the measured ion count rate.

The constant signal level of about $5 \cdot 10^{-3}$ per bin per laser shot in Fig. 2 is attributed to ionization fragments from residual gas molecules embedded in the helium nanodroplets. At low pulse energy (2 mJ), a small signal peak at about 1.6 ms time of flight is recorded indicating laser induced doping of the droplets with Mg atoms. At high pulse energy (100 mJ), the ion signal is completely depleted in the time interval, in which a positive doping signal was previously measured. Clearly, the droplet beam is destroyed due to the interaction with a dense ablation plume. The width of the signal minimum of about 80 μ s corresponds to the length of the droplet beam interval which is exposed to the expanding plasma plume of 15 mm when taking time-of-flight broadening into account. However, both at earlier and at later times doping of the droplet beam prevails. The fact that significant doping takes place up to 1 ms after the attenuation phase is explained by the ablated particles undergoing multiple scattering events before being decelerated and sticking to the droplets [8]. The small positive doping signal at earlier times (1.7 ms) might stem from weak doping before a high particle density has built up to deplete the droplet beam or it might be due to Mg atoms being forward scattered in the direction of the helium beam through the skimmer and being picked up further downstreams. A clear signal of forward scattered Mg ions has been observed in earlier experiments in time-of-flight spectra of ion-doped helium droplets.

Using the QMS as a detector has the advantage of allowing mass-selective measurements of the yield of monomers and oligomers of the laser-doped material. Typical time-of-flight signal traces recorded at the mass of the Mg monomer, dimer and trimer using laser ablation with the Nd:YLF laser (526 nm) with a pulse energy of 6.3 mJ at 1 kHz repetition rate are depicted in the inset of Fig. 3. The signal-to-noise ratio is much better than the one of Fig. 2 as a result of averaging over 10^5 laser

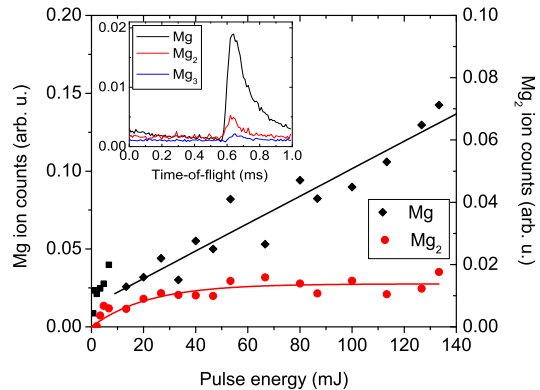


FIG. 3: Dependence of the yield of ionized Mg monomers and dimers as a function of laser pulse energy. Inset: Time-of-flight signal traces of Mg doped droplets recorded at the mass of the Mg monomer, dimer and trimer.

shots and due to the better shot-to-shot stability of the pulse energy of the Nd:YLF laser. Despite of maximum focusing of the laser beam, destruction of the droplet beam at this pulse energy is barely visible as a small dip of the ion yield right before the doping signal maxima. Note the falling level of the monomer signal from 0 to 0.6 ms, which is due to doping by the previous laser shot. Thus, at an ablation rate of 1 kHz nearly continuous doping of the droplet beam is achieved.

In order to investigate the efficiency of multiple doping at higher pulse energies similar measurements using the 10 Hz Nd:YAG laser are carried out. Fig. 3 shows the yield of monomers versus dimers for pulse energies up to 140 mJ. The plotted ion count rate is obtained by integrating the count rate over an interval of width 200 μ s. The curved solid line represents the fit of a simple saturation model and is intended to guide the eye. Note the different vertical scales for monomer and dimer signals (left and right, respectively). One observes a local maximum both of monomer and dimer doping at low energies between 5 and 10 mJ, similar to doping with Li. This observation will be discussed in more detail in the following section. At higher pulse energies, the monomer yield again increases roughly linearly, as indicated by the straight line. However, the dimer signal saturates at about 50 mJ at an ion count rate of 0.015 counts per laser shot and thus always stays well behind the monomer signal. The same behavior has been observed with all metal samples discussed below. Thus we conclude that the pick-up process in the laser ablation plume proceeds in a significantly different way from the one in the vapor inside a heated oven, which is known to follow Poissonian statistics [24]. Although the relative intensities may be perturbed by fragmentation processes upon electron impact ionization we don't expect larger cluster masses to disappear completely [4].

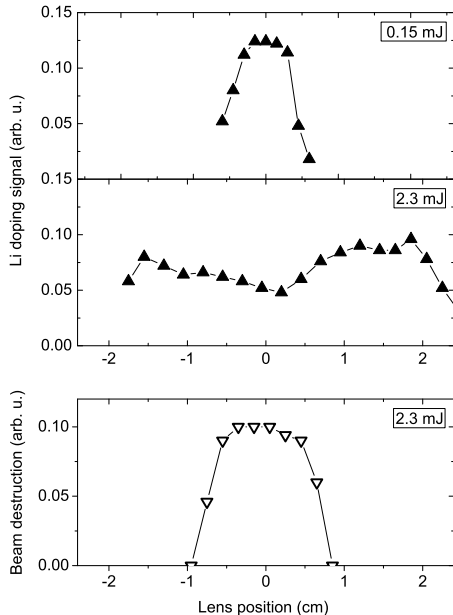


FIG. 4: Amplitude of the doping signal as a function of the position of the focusing lens for low (0.15 mJ) (a) and moderate (2.3 mJ) (b) pulse energies. Amplitude of the signal drop due to beam destruction at moderate (2.3 mJ) pulse energies (c).

B. Laser ablation of lithium

Systematic experiments for characterizing the new laser ablation setup are carried out using solid Li as sample material for several reasons. Alkali atoms and clusters are very sensitively detected by a Langmuir-Taylor (LT) surface ionization detector [22]. From previous experiments it is known that alkali metals are efficiently ablated at low laser intensities. Li atoms are easily accessible by electronic spectroscopy using dye lasers and the spectrum of Li attached to helium nanodroplets is well known [25]. Furthermore, Li can be purchased as metal rods 10 mm in diameter and can be handled with reasonable safety measures.

The measured signal traces are very similar to the ones recorded with Mg, the only difference being additional broadening due to the response time of the LT-detector of about 50 μ s. The amplitude of the signal maxima resulting from laser-doping at two different laser pulse energies, 0.15 mJ and 2.3 mJ, is represented in Fig. 4 (a) and (b), respectively, as a function of the position of the 300 mm focusing lens. The waist of the laser beam in the focus was measured to be $w_0 = 36 \mu$ m and at 1 cm displacement it is $w = 160 \mu$ m. At low pulse energy the doping efficiency is clearly peaked around the focus position (Fig. 4 (a)). However, at higher pulse energy maximum doping is achieved when the lens is shifted along the beam by about 1-2 cm to either direction out of the

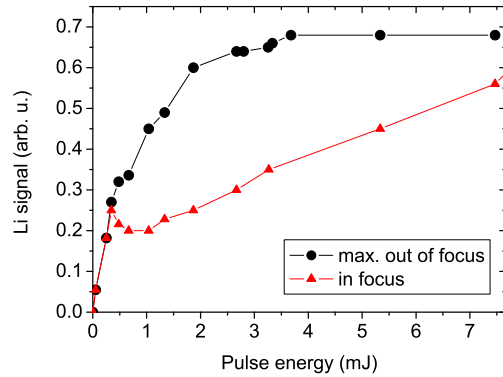


FIG. 5: Amplitudes of the laser doping signal as a function of laser pulse energy at the lens position of the maximum doping by desorption (circles) and in focus (triangles).

focus position (Fig. 4 (b)). This behavior reflects the fact that for maximum focusing destruction of the beam partially compensates for higher doping efficiency, whereas outside the focus position, where energy density is low, only doping occurs. Thus, two distinct regimes of laser-matter interaction appear to be active: At low energy density, vaporization of material into the gas phase with low kinetic energy transfer occurs. In this regime, a luminescent plasma at the laser – rod interaction point is barely visible. At higher energy density, in contrast, a bright plasma plume can be seen. In this regime, the ejected material acquires large kinetic energy, presumably due to more violent interactions inside the strongly ionized plasma.

Fig. 4 (c) displays the beam depletion due to the laser ablated material as a function of lens position at 2.3 mJ pulse energy. Clearly, the maximum signal drop is correlated with the local minimum of the doping signal shown in Fig. 4 (b). The steep edges of both the doping maximum in Fig. 4 (a) and the depletion maximum in Fig. 4 (c) indicate that both processes exhibit a threshold behavior as a function of laser energy, however, with different threshold values.

Fig. 5 depicts the doping signal amplitudes at the focus position (triangles) and at the position of maximum doping efficiency outside the focus (dots). Strikingly, at about 0.3 mJ pulse energy beam destruction suddenly sets in for the case of tight focusing. With increasing pulse energy, the doping signal even decreases to a local minimum at about 1 mJ before rising again almost linearly. As mentioned in the previous section, a similar behaviour occurs when ablating Mg. The doping signal continuously increases even when the laser pulse energy goes up to 200 mJ, as observed using the 10 Hz Nd:YAG laser. Thus, the density of particles amenable to pick-up by helium droplets by scattering with helium gas further increases. In this regime of laser ablation, large amounts

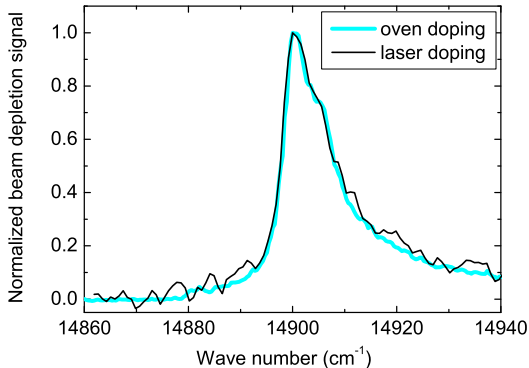


FIG. 6: Spectrum of helium nanodroplets doped with Li atoms by means of laser ablation (red line) in comparison with oven doping.

of material are ejected into the gas phase which can be seen from the fast rate of removal of material from the sample and from coating of the laser entrance window. The doping amplitude at the lens position of most efficient doping outside the focus (vaporization), however, continuously increases before saturating. From analyzing the dependence of peak position and pulse energy we find that maximum doping by vaporization is correlated with a constant energy density per pulse of 50 J/cm^2 in the case of ablating Li, which is nearly independent of the diameter of the laser spot on the sample surface. The initial signal rise is then explained by a growing effective surface area from which the atoms are vaporized. As the laser waist on the surface reaches 0.3 mm at about 3 mJ pulse energy, the density of vaporized slow Li atoms becomes sufficiently high that the droplet beam is attenuated by multiple pick-up of atoms. Besides, at this size of the laser spot the finite curvature of the sample surface is expected to play a role. Thus, for laser doping using moderate pulse energies in the range of $0.5\text{--}10 \text{ mJ}$, which are typical for kHz lasers, optimal conditions are obtained when defocusing the laser beam on the sample to a waist of $0.1\text{--}0.5 \text{ mm}$.

The objective of implementing a kHz laser ablation source into our apparatus is to carry out electronic spectroscopy of atoms, molecules, and ions inside helium droplets, which are not amenable to doping by evaporation in an oven. As a first demonstration experiment, the beam depletion spectrum of the D2 atomic transition of Li attached to helium droplets is measured with laser doped Li and, for comparison, with Li doped using a conventional oven. The resulting spectra are depicted in Fig. 6. In the experiment, the beam of a cw dye laser is superimposed coaxially with the helium droplet beam ($\approx 50 \text{ mW}$ laser power coupled into the machine). The depletion of the doped helium droplet beam upon electronic excitation is measured with the LT-detector. The

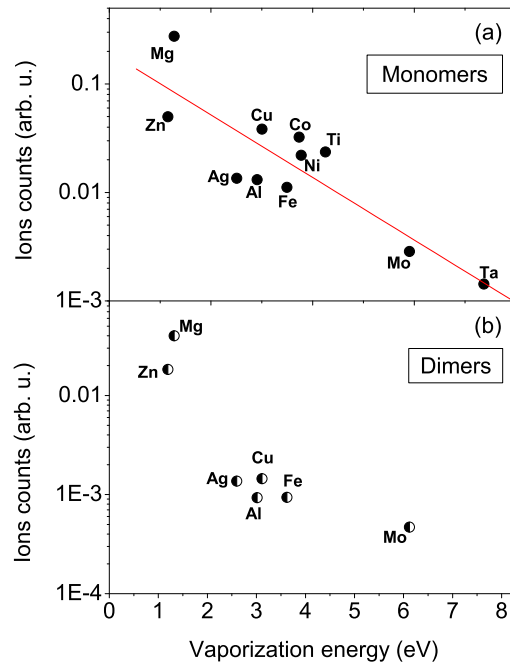


FIG. 7: Yield of various metal monomers (a) and dimers (b) detected by the QMS as a function of vaporization energy [26].

two spectra nicely match. However, the signal-to-noise ratio for ablation-doped Li is much lower with respect to oven-doping. One reason is the given lower duty-cycle of about 10% for laser doping. Secondly, since the laser doping has not been optimized for picking up one atom per droplet only, the LT detector signals also have contributions from lithium oligomers which do not show up in the observed depletion spectrum. Finally, shot to shot fluctuations diminish signal to noise ratios. In our case Li samples do not have a perfectly flat surface since we are dealing with a soft material that has to be cleaned by scraping off the oxidized surface layer with a knife prior to mounting onto the sample coupler. Consequently, for the harder metal samples discussed below, shot-to-shot fluctuations are found to be smaller although the absolute signal rates are lower.

C. Doping with non-volatile metals

In order to test the new ablation setup for doping helium nanodroplets with high temperature refractory materials, a variety of metal samples have been tried out. On the one hand, the ability of doping helium nanodroplets with pure metal atoms is of interest for extending the panoply of systems for spectroscopic studies. Moreover, compounds of organic molecules and metal atoms are of considerable interest for potential applica-

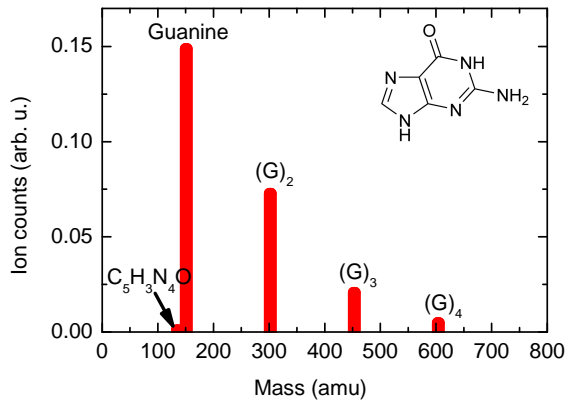


FIG. 8: Yield of guanine and guanine oligomers doped in helium nanodroplets by laser ablation.

tions as catalysts. On the other hand, the isolation of metal clusters inside helium droplets at a temperature of 0.4 K would open the way to studying the magnetic and superconducting properties of such nano-sized systems.

Fig. 7 gives an overview over the metals studied so far. The laser is operated at maximum pulse energy of about 10 mJ and the beam focus is placed onto the sample surface. The yield of ionized monomers and dimers detected by the QMS is represented in a logarithmic scale as a function of the vaporization energy in Fig. 7 (a) and (b), respectively. The plotted ion counts reflects the average number of detected ions per laser shot within a time window of 200 μ s. The different detection efficiencies for the different masses are not corrected for. The straight line in Fig. 7 (a) represents the fit of an exponentially decreasing function to indicate the general trend as observed with these selected metals. The efficiency of doping helium droplets with tantalum is more than 2 orders of magnitude lower than for doping with Mg. Fig. 7 (b) shows only those materials for which a significant dimer signal was measured. This is not the case for copper, cobalt, nickel, titanium, and tantalum. Obviously, the ablation efficiency does not merely depend on the vaporization energy, but is related in a complex fashion to a number of parameters including heat capacity, heat conductivity, reflectivity of the surface, absorption spectrum of ablated atoms, etc. The important point here is that all materials tested so far can be laser ablated and lead to a measurable doping signal. No significant formation yield of metal clusters has been achieved in our experiments. However, parameters like e.g. the droplet size distributions, which has been shown to influence significantly multiple pickup, has not been optimized for metal cluster formation so far.

D. Doping with biomolecules

Doping helium nanodroplets with biomolecules is of considerable interest in the context of matrix isolation

spectroscopy and photobiology at very low temperatures [27]. Thermalization of large molecules to the equilibrium temperature of helium nanodroplets of 0.4 K is known to tremendously simplify the structure of the spectra with only negligible perturbation due to the interaction of the molecule with the helium environment [28, 29]. The neat DNA base guanine is used as the first demonstration system. As for many biomolecules, simple heating would lead to thermal decomposition before vaporization [30]. Laser desorption of guanine at high repetition rate was also demonstrated by Smits *et al.* [23].

The sample is prepared by pressing neat guanine into cylindrical shape onto a threaded rod. Fig. 8 displays the yield of guanine monomers and oligomers as detected by the QMS. The laser pulse energy is set to 1.5 mJ at maximum focusing of the laser beam. Under these conditions, laser desorption at 1 kHz repetition rate is stable for more than one hour. The count rate of the monomer signal is found to be comparable to the one achieved by Smits *et al.* using femtosecond resonant photoionization. Only negligible fragmentation is observed, the largest fragment contribution being $C_5H_3N_4O$ at a mass of 135 amu with only 0.7 % of monomer signal. The relative yields of dimers, trimers and tetramers is found to be slightly larger compared to the observations of Smits *et al.* This is quite surprising given the fact that clustering of metal atoms was found to be much less efficient in our experiment but may be due to the larger droplet sizes used.

With laser desorption of guanine, the maximum signal yield is obtained for a nozzle temperature of 14 K and a stagnation pressure of 54 bar which corresponds to expansion conditions close to the transition to the expansion out of liquid helium (supercritical expansion). At these source conditions, the average number of helium atoms per droplet is expected to lie in the range $1\text{-}2\cdot 10^4$. The need for large helium droplets is attributed to the fact that large molecules such as guanine carry large amounts of internal energy due to their large number of internal degrees of freedom. Consequently, cooling to 0.4 K requires the ability of the droplets to evaporate a large number of helium atoms.

E. Laser evaporation of carbon samples

Besides pressing samples of neat material, large organic molecules are commonly prepared in samples consisting of the molecules and a matrix material. Since the standard matrix material for laser desorption is graphite we chose neat graphite as another material for testing our setup.

Typical QMS count rates measured at different oligomer masses are depicted in Fig. 9. The monomer signal is not shown because of a large background count rate at the mass of 12 amu which stems from the ionization of hydrocarbons in the residual gas of the vacuum system and from He_3^+ fragments. An upper limit for the

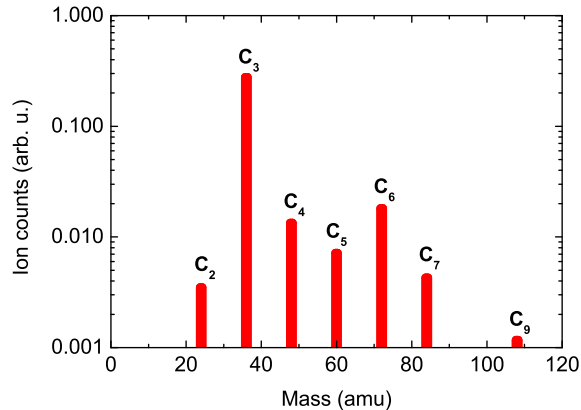


FIG. 9: Yield of small carbon clusters doped in helium nanodroplets by ablation of a graphite sample.

monomer signal rate can be estimated to 0.05 events per laser shot. C_3^+ is by far the dominating cluster size with a count rate of 0.3 s^{-1} . This is the highest count rate of all materials studied so far. This observation is consistent with earlier measurements on the fragmentation of small carbon clusters [31, 32]. It is due to the local stability of C_3 and C_3^+ clusters [33]. As for doping with guanine, the highest yield of carbon oligomers is obtained at considerably lower nozzle temperatures (19 K for C_2 , 18 K for C_3 , 15 K for C_4 , and 14 K for C_5 , C_6 , C_7 , C_8).

In this case we interpret the need for large helium droplets by the large amount of binding energy (6.4, 13.9, 19.0, 26.3, 31.8, 38.7, 44.3, 51.0 eV for neutral clusters C_n , where n runs from 2 to 9, respectively) liberated upon cluster formation during the interaction of carbon atoms with helium [33]. Despite the high signal yield obtained at maximum laser power and tight focusing, the sample surface is only weakly degraded after more than 2 hours of laser ablation at 1 kHz repetition rate. The laser entrance window remained nearly uncoated, such that the laser-doping signal rate was stable for many hours of operation.

IV. SUMMARY

In conclusion we demonstrated that helium nanodroplets can be doped quite efficiently by means of laser ablation at kHz repetition rates. The method is characterized in terms of laser fluences, focussing conditions, etc. For the first time, metals have been doped for which thermal evaporation is not an option. The intensities of doping the different materials are compared quantitatively. Extending the doping method to biomolecules, attachment of guanine to helium droplets has been demonstrated. The unfragmented monomers as well as oligomers have been observed. Finally, graphite

samples provide as all the other materials stable evaporation conditions. In combination with other organic samples this opens the possibility to use matrix assisted laser desorption to extend studies at ultracold temperatures in helium droplets to a variety of molecules of biological interest.

V. ACKNOWLEDGEMENTS

The authors gratefully acknowledge stimulating discussions with A. Stolow and J. Tiggesbäumker and financial support by the Deutsche Forschungsgemeinschaft.

-
- [1] J. P. Toennies and A. F. Vilesov, *Angewandte Chemie* **43**, 2622 (2004).
- [2] S. Grebenev, B. G. Sartakov, J. P. Toennies, and A. F. Vilesov, *J. Chem. Phys.* **114**, 617 (2001).
- [3] S. Grebenev, E. Lugovoi, B. G. Sartakov, J. P. Toennies, and A. F. Vilesov, *J. Chem. Phys.* **118**, 8217 (2000).
- [4] J. Tiggesbäumker and F. Stienkemeier, *Phys. Chem. Chem. Phys.* **9**, xxxx (2007).
- [5] F. Stienkemeier and K. Lehmann, *J. Phys. B* **39**, R127 (2006).
- [6] F. Stienkemeier and A. F. Vilesov, *J. Chem. Phys.* **115**, 10119 (2001).
- [7] J. Küpper, J. M. Merritt, and R. E. Miller, *J. Chem. Phys.* **117**, 647 (2002).
- [8] P. Claas, S.-O. Mende, and F. Stienkemeier, *Rev. Sci. Instr.* **74**, 4071 (2003).
- [9] D. E. Galli, M. Buzzacchi, and L. Reatto, *J. Chem. Phys.* **115**, 10239 (2001).
- [10] M. A. Posthumus, P. G. Kistemaker, H. L. C. Meuzelaar, and M. C. T. N. de Brauw, *Annal. Chem.* **50**, 985 (1978).
- [11] M. Karas, D. Bachmann, U. Bahr, and F. Hillenkamp, *Int. J. Mass. Spectrom. Ion Processes* **78**, 53 (1987).
- [12] R. J. Levis, *Annu. Rev. Phys. Chem.* **45**, 483 (1994).
- [13] D. E. Powers, S. G. Hansen, M. E. Geusic, D. L. Michalopoulos, and R. E. Smalley, *J. Chem. Phys.* **78**, 2866 (1983).
- [14] K. LaiHing, R. G. Wheeler, W. L. Wilson, and M. A. Duncan, *J. Chem. Phys.* **87**, 3401 (1987).
- [15] P. Milani and W. A. deHeer, *Rev. Sci. Instr.* **61**, 1835 (1990).
- [16] U. Heiz, F. Vanolli, L. Trento, and W.-D. Schneider, *Rev. Sci. Instr.* **68**, 1986 (1997).
- [17] R. L. Wagner, W. D. Vann, and J. A. W. Castleman, *Rev. Sci. Instr.* **68**, 3010 (1997).
- [18] H. Haberland, *Clusters of Atoms and Molecules* (Springer Series in Chemical Physics (Springer Berlin), 1994).
- [19] V. Ghazarian, J. Elorata, and V. A. Apkarian, *Rev. Sci. Instr.* **73**, 3606 (2002).
- [20] J. W. Elam and D. H. Levy, *J. Phys. Chem. B* **102**, 8113 (1998).
- [21] F. Stienkemeier, F. Meier, and H. O. Lutz, *Eur. Phys. J. D* **9**, 313 (1999).
- [22] F. Stienkemeier, M. Wewer, F. Meier, and H. O. Lutz, *Rev. Sci. Instr.* **71**, 3480 (2000).
- [23] M. Smits, C. A. de Lange, S. Ullrich, T. Schulz, M. Schmitt, J. G. Underwood, J. P. Shaffer, D. M. Rayner, and A. Stolow, *Rev. Sci. Instr.* **74**, 4812 (2003).
- [24] M. Lewerenz, B. Schilling, and J. P. Toennies, *J. Chem. Phys.* **102**, 8191 (1995).
- [25] F. Stienkemeier, J. Higgins, C. Callegari, S. I. Kanorsky, W. E. Ernst, and G. Scoles, *Z. Phys. D* **38**, 253 (1996).
- [26] www.periodensystem.info.
- [27] A. H. Zewail, *J. Phys. Chem. A* **104**, 5660 (2000).
- [28] A. Lindinger, J. P. Toennies, and A. F. Vilesov, *J. Chem. Phys.* **110**, 1429 (1999).
- [29] F. Huysken, O. Werhahn, A. Y. Ivanov, and S. Krasnokutski, *J. Chem. Phys.* **111**, 2978 (1999).
- [30] F. Piuze, I. Dimicoli, M. Mons, B. Tardivel, and Q. Zhao, *Chem. Phys. Lett.* **320**, 8381 (2000).
- [31] E. A. Rohlfing, D. M. Cox, and A. Kaldor, *J. Chem. Phys.* **81**, 3322 (1984).
- [32] R. Ramanathan, J. A. Zimmerman, and J. R. Eyler, *J. Chem. Phys.* **98**, 7838 (1993).
- [33] K. Raghavachari and J. S. Binkley, *J. Chem. Phys.* **87**, 2191 (1987).